Korean J. Chem. Eng., **21**(5), 983-988 (2004)

The Effects of Ni Doping on the Performance of O3-Lithium Manganese Oxide Material

Ki Soo Park, Myung Hun Cho, Sung Jang Jin, Chi Hoon Song and Kee Suk Nahm†

School of Chemical Engineering and Technology, College of Engineering,
Chonbuk National University, Chonju 561-756, Korea
(*Received 2 March 2004 • accepted 29 April 2004*)

Abstract–$Li_{0.7}[Li_{1/6}Mn_{5/6}]O_2$ and $Li_{0.7}[Li_{1/12}Ni_{1/12}Mn_{5/6}]O_2$ powders were synthesized by a sol-gel method. The powders had a typically rhombohedral layered O3 structure. Both the samples were nanometer-sized powders and the size of $Li_{0.7}[Li_{1/12}Ni_{1/12}Mn_{5/6}]O_2$ was smaller than that of $Li_{0.7}[Li_{1/6}Mn_{5/6}]O_2$. The discharge curve shape of both the sample electrodes was almost equal to that of the layered structure. However, the electrode materials were transferred from layered to spinel structures with increasing the cycle number. $Li/Li_{0.7}[Li_{1/6}Mn_{5/6}]O_2$ and $Li_{0.7}[Li_{1/12}Ni_{1/12}Mn_{5/6}]O_2$ cells initially delivered a discharge capacity of 261 and 238 mAh/g, respectively. The capacities of $Li/Li_{0.7}[Li_{1/6}Mn_{5/6}]O_2$ and $Li_{0.7}[Li_{1/12}Ni_{1/12}Mn_{5/6}]O_2$ after the 45th cycle were 174 and 221 mAh/g, respectively, corresponding to the retentions of 67% and 93%. The nanostructure of the synthesized powders seems to result in high initial discharge capacity as well as in the suppression of the discharge capacity fading by providing high surface area needed for Li ion reaction. In Ni doped-$Li_{0.7}[Li_{1/12}Ni_{1/12}Mn_{5/6}]O_2$, the capacity fading was reduced by suppressing the oxidation state of Mn from 4^+ to 3^+ due to the role of Ni ion doped.

Key words: Sol-gel Method, Ni Doping, Layered Structure, Nanostructure, Nanograin

INTRODUCTION

Layered oxide materials, such as $LiCoO_2$ [Kang et al., 1999; Holzapel et al., 2001], $LiNiO_2$ [Park et al., 2001, 2002], and $LiMnO_2$ [Davidson et al., 1995; Crohuennec et al., 1997], have been studied as cathode materials for Li-ion batteries. The layered oxide materials with $LiMO_2$ formula derived high discharge capacity. However, these materials have the disadvantages of high cost and toxicity for $LiCoO_2$ [Armstrong et al., 1998], of thermal instability and nonstoichiometric synthesis for $LiNiO_2$ [Lee et al., 1999], and of drastic capacity fading due to phase transition for $LiMnO_2$ [Paulsen et al., 2000]. Therefore, many researchers have attempted to develop new materials that are environmental benign, low cost, and have high discharge capacity. Although capacity fading of $LiMnO_2$ rapidly progresses, the $LiMnO_2$ is a proper material for this demand. Many researchers have studied cation doping of Cr [Davidson et al., 1999], Al [Ammundsen et al., 1996], Co [Bruce et al., 1999], and Ni [Armstrong et al., 2002] for Mn site to suppress the capacity fading of $LiMnO_2$. These efforts showed a decrease of the capacity fading, but any investigation to reveal the reason why these metals suppress the capacity fading is still insufficient. The synthesis of layered Li_xMnO_2 with an O2 structure has been studied by Dahn's group using a solid-state reaction [Paulsen et al., 1999, 2000; Lu et al., 2000]. They first prepared layered $Na_{0.7}[M_{1/3}Mn_{2/3}]O_2$ with stoichiometric amounts of Mn_2O_3, Li_2CO_3, and Na_2CO_3 using a solid state-reaction, and then ion-exchanged the prepared P2-$Na_{0.7}[M_{1/3}Mn_{2/3}]O_2$ in a boiling solution of 5 M lithium bromide dissolved in hexanol to form the layered O2 structure. They observed that the O2 structure showed the best discharge capacity of about 170 mAh/g [Paulsen et al., 2000]. They also reported the doping effects of Li, Ni, and Co. However, the charge/discharge curve differed from existing layered $LiNiO_2$, $LiCoO_2$, etc. The curve shape had two plateaus as shown in spinel structure. On the other hand, Bruce et al. [1999] asserted that the charge/discharge cycling of the synthesized powders induces the formation of nanostructured grain in the particles, which suppresses capacity loss, even though there is expansion/contraction of the lattice and phase transitions during the cycle. There are still some debates on the mechanism of capacity fading inhibition by cation doping.

In this work, therefore, we synthesized $Li_{0.7}[Li_{1/6}Mn_{5/6}]O_2$ and $Li_{0.7}[Li_{1/12}Ni_{1/12}Mn_{5/6}]O_2$ using a sol-gel method to investigate the mechanism of capacity fading suppression. Sodium manganese bronze precursors were first synthesized by a sol-gel method, and then the lithium manganese oxides were prepared by an ion exchange of Li for Na in the sodium manganese bronze precursors. Structural properties of the prepared materials were characterized by using XRD, SEM, and particle size analyzer. The electrochemical properties of the materials were also investigated to observe the effect of cation doping and grain size.

EXPERIMENT

$Na_{0.7}[Li_{1/6}Mn_{5/6}]O_2$ precursor was synthesized by using a sol-gel method as previously reported [Sun et al., 1998, 1999, 2002; Park et al., 2002]. Sodium acetate (CH_3CO_2Na, Aldrich), lithium acetate ($Li(CH_3COO)\cdot 2H_2O$), and manganese acetate ($Mn(CH_3COO)\cdot 4H_2O$) were employed as starting materials. Stoichiometric amounts of the sodium, lithium, and manganese acetate salts were dissolved in DI water with a cationic ratio of Na : Li : Mn=0.7 : 1/6 : 5/6. The dissolved solution was added dropwise into continuously agitating aqueous adipic acid. The molar ratio of chelating agent to total metal ions was fixed at unity. The prepared solution was evaporated at 70-80 °C for 5 hrs until a transparent sol was obtained. As water

†To whom correspondence should be addressed.
E-mail: nahmks@moak.chonbuk.ac.kr

evaporated further, the sol turned into a viscous transparent gel. The resulting gel precursors were heated with a ramping rate of 1 °C/min and decomposed at 450 °C for 10 hrs in air to eliminate organic components. Thus obtained powders were calcined at 700 °C in a flow of air for 10 hrs. After the calcination process, the powders were suddenly quenched in liquid nitrogen. In the case of $Na_{0.7}[Li_{1/12}Ni_{1/12}Mn_{5/6}]O_2$ precursor preparation, all the process was the same except that nickel acetate ($Ni(CH_3COO)_2 \cdot 4H_2O$) and lithium acetate ($Li(CH_3COO) \cdot 2H_2O$) were used instead of employing lithium acetate ($Li(CH_3COO) \cdot 2H_2O$) only. Stoichiometric amount of sodium, lithium, nickel acetate, and manganese acetate salts was Na : Li : Ni : Mn=0.7 : 1/12 : 1/12 : 5/6.

The prepared precursor powders (5 g) were introduced into a mixed solution of hexanol (150 ml) and lithium bromide (LiBr; 55 g). The ion exchange of Li for Na in $Na_{0.7}[Li_{1/6}Mn_{5/6}]O_2$ and $Na_{0.7}[Li_{1/12}Ni_{1/12}Mn_{5/6}]O_2$ was carried out at 160 °C for 3 hrs under air environment in a batch reactor equipped with a reflux condenser. After the reaction, the solution was filtered by using an aspirator under vacuum, and the remaining powders were washed with methyl alcohol. The washed powders were dried at 180 °C for 10 hrs in a vacuum oven. After the synthesis, the structure of the prepared powders was characterized by using powder X-ray diffraction (XRD, D/Max-3A, Rigaku) with a Cu-Kα radiation. The particle size of the prepared sample powders was measured by a Particle and Pore Size Analysis System (Particle Size Analyzer : UPA-150).

The electrochemical characterization was carried out by using CR2032 coin-type cells. The test cells were assembled by the following method: the cathode was fabricated with an accurately weighed active material (20 mg) and conductive binder (13 mg). It was pressed on 25 mm^2 stainless steel mesh used as the current collector at 300 kg/cm^2 and dried at 200 °C for 5 hrs in an oven. The cell was composed of a cathode and a lithium metal anode (Cyprus Foote Mineral Co.) separated by a porous polypropylene film (Celgard 3401). The electrolyte was a mixed solution of 1 M $LiPF_6$-ethylene carbonate (EC)/dimethyl carbonate (DMC) (1 : 2 by volume). The cells were assembled in an argon-filled dry box and tested at room temperature. The cell was charged and discharged at a current density of 0.8 mA/cm^2 in the voltage range of 2.0-4.6 V (vs. Li/Li^+).

RESULT AND DISCUSSION

Fig. 1(a) and (b) show the XRD patterns of $Na_{0.7}[Li_{1/6}Mn_{5/6}]O_2$ and $Na_{0.7}[Li_{1/12}Ni_{1/12}Mn_{5/6}]O_2$ powders, respectively, synthesized at 700 °C using adipic acid. Both the samples show almost similar XRD spectra. The synthesized materials are considered to have a symmetric P3 structure partially mingled with P2 phase. All the samples show a (002) plane at 2θ=16°, which results from Na ion and indexed P2 structure with a symmetric hexagonal space group structure ($P6_3/mmc$). The spectra show some impurity related peaks, shown with an asterisk. The characteristic peaks spectra of the P3 structure are observed at 2θ=36.5, 37.5, 45.5, 53, and 57 with other small peaks at 2θ=32, 64, 67, and 74, whereas a typical XRD spectrum of P2 structure includes (012), (013) and (014) planes at 2θ=39.5, 44, and 49°, respectively, as characteristic peaks with other low intensity peaks observed at 2θ=32, 36, 62, 65, 67, 74. Accordingly, it becomes apparent that our synthesized $Na_{0.7}[Li_{1/6}Mn_{5/6}]O_2$ and $Na_{0.7}[Li_{1/12}Ni_{1/12}Mn_{5/6}]O_2$ have P3 structure partially mingled with P2 phase.

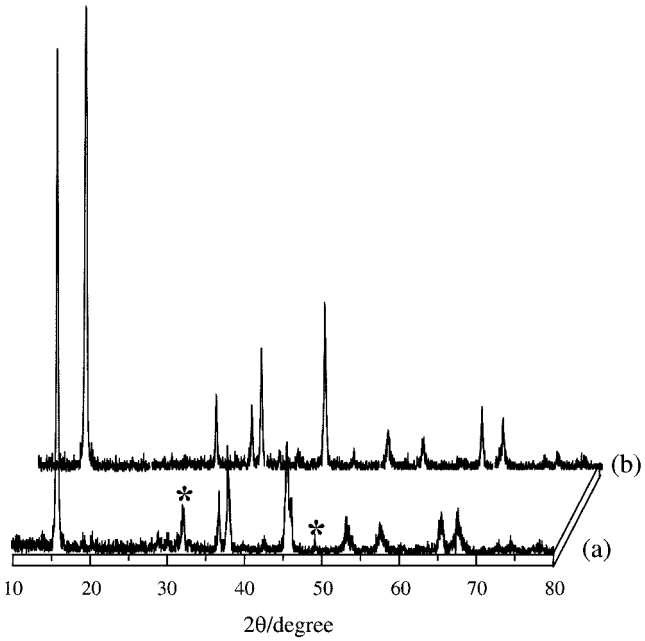

Fig. 1. XRD spectra for (a) $Na_{0.7}[Li_{1/6}Mn_{5/6}]O_2$ and (b) $Na_{0.7}[Li_{1/12}Ni_{1/12}Mn_{5/6}]O_2$ powders synthesized at 700 °C using adipic acid.

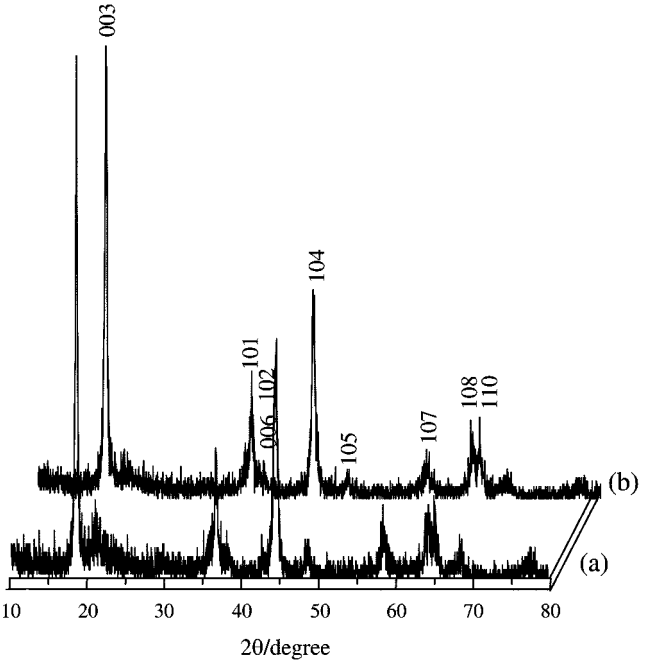

Fig. 2. XRD spectra for (a) $Li_{0.7}[Li_{1/6}Mn_{5/6}]O_2$ and (b) $Li_{0.7}[Li_{1/12}Ni_{1/12}Mn_{5/6}]O_2$ prepared by ion exchange of $Na_{0.7}[Li_{1/6}Mn_{5/6}]O_2$ and $Na_{0.7}[Li_{1/12}Ni_{1/12}Mn_{5/6}]O_2$, respectively.

Shown in Fig. 2(a) and (b) are the XRD patterns of $Li_{0.7}[Li_{1/6}Mn_{5/6}]O_2$ and $Li_{0.7}[Li_{1/12}Ni_{1/12}Mn_{5/6}]O_2$, respectively, prepared by ion exchange of $Na_{0.7}[Li_{1/6}Mn_{5/6}]O_2$ and $Na_{0.7}[Li_{1/12}Ni_{1/12}Mn_{5/6}]O_2$. A perfect ion exchange was accomplished for both the samples without the formation of impurities. The peak (2θ=16°) resulting form Na ion thoroughly disappears, whereas the peak (2θ=18°) from Li ion appears from the XRD spectra. This indicates that the ion exchange of

Li for Na in the sodium manganese bronzes is successfully achieved in this work. As-prepared samples show typical rhombohedral O3 layered structure. XRD patterns of the $Li_{0.7}[Li_{1/6}Mn_{5/6}]O_2$ and $Li_{0.7}[Li_{1/12}Ni_{1/12}Mn_{5/6}]O_2$ are similar to those of $Li(Mn_{1-y}Co_y)O_2$ synthesized by Bruce et al. [1999]. The patterns are also analogous to that of spinel structure. Lu et al. [Lu and Dahn, 2002], Thackeray [1997], and Choi et al. [Choi and Manthiram, 2002] reported that O3 layered and spinel structures have a similarity in XRD peak positions and relative intensities. The O3 structure shows the splitting of a peak at $2\theta=37^o$ into (006) and (102) as well as that at $2\theta=64^o$ into (018) and (110), whereas the peaks (002) and (440), respectively, at $2\theta=37^o$ and 66^o present only one peak at each position for spinel structure. When we compare the results of above literatures with XRD data in Fig. 2, it is considered that our prepared samples are O3 structure.

One of the classification methods to distinguish O3 from spinel structure is in comparison with lattice constants of the materials. It has been reported that a material with c/a ratio of 4.9 in rhombohedral symmetry is equivalent to a cubic cell. If c/a>4.9, the material is not the cubic cell [Bruce et al., 1999; Armstrong et al., 1999]. We measured lattice constants of as-prepared samples by using Rietveld method. Lattice parameters, a and c, were 2.88 and 14.47, respectively, for $Li_{0.7}[Li_{1/6}Mn_{5/6}]O_2$ and were 2.91 and 14.99, respectively, for $Li_{0.7}[Li_{1/12}Ni_{1/12}Mn_{5/6}]O_2$. The c/a ratios of $Li_{0.7}[Li_{1/6}Mn_{5/6}]O_2$ and $Li_{0.7}[Li_{1/12}Ni_{1/12}Mn_{5/6}]O_2$ were 5.02 and 5.15, respectively. The c/a ratios of as-prepared samples are higher than that of cubic spinel structure. This means that our prepared samples are O3 structure, but not spinel structure. The XRD patterns of Fig. 2 also show the broad characteristic peaks with low intensities, which seems to be originated from stacking faults in the synthesized materials. Paulsen et al. reported that the broad characteristic peaks with low intensities are ascribed to layer gliding effect occurred in the layered structure when the structure changes from P2 to O2 during ion exchange [Paulsen et al., 1999, 2000]. Meanwhile, Rovertson et al. explained that the broad peaks reflect the presence of the nanostructure within the particles [Robertson et al., 2001]. They suggested that the increase of the peak broadening is due to unclear demarcation between ordered and disordered vacancies or different form of layered stacking. Therefore, it is thought that the XRD peak broadening of as-prepared samples is due to the presence of nanostructure within the particles and the different form of layered stacking.

Fig. 3(a) and (b) show SEM images for $Li_{0.7}[Li_{1/6}Mn_{5/6}]O_2$ and $Li_{0.7}[Li_{1/12}Ni_{1/12}Mn_{5/6}]O_2$ powders. Both the samples show the nanometer-sized powders. It is thought that the synthesis of nanometer-sized powders is achieved at relatively lower temperature by using a sol-gel method, which is easy to control the size down to atomic level. It was reported that the sol-gel method is effective to control the particle size down to atomic level [Lee et al., 1999]. The particle size of $Li_{0.7}[Li_{1/12}Ni_{1/12}Mn_{5/6}]O_2$ is more small (300 nm) and uniformly dispersed than that of $Li_{0.7}[Li_{1/6}Mn_{5/6}]O_2$ (500 nm). We speculated that the difference in particle size between the two samples could be explained by using the differences of binding energy and ion-radii of elements constituting the materials. The binding energy difference of Ni and Mn (115.2 eV) is larger than that of Li and Mn (101.9 eV) [Lide, 1997]. A strong binding energy might shrink the particle size, resulting in the formation of smaller $Li_{0.7}[Li_{1/12}Ni_{1/12}Mn_{5/6}]O_2$ powders. However, ionic radius of Li+ and Ni 2+ are 0.68 Å and 0.69 Å [Lide, 1997.], respectively, which is not a big difference in the radius. Therefore, we speculate that the particle size of the samples is not seriously affected by ionic radius, but is greatly influenced by the binding energy difference of the constituting elements.

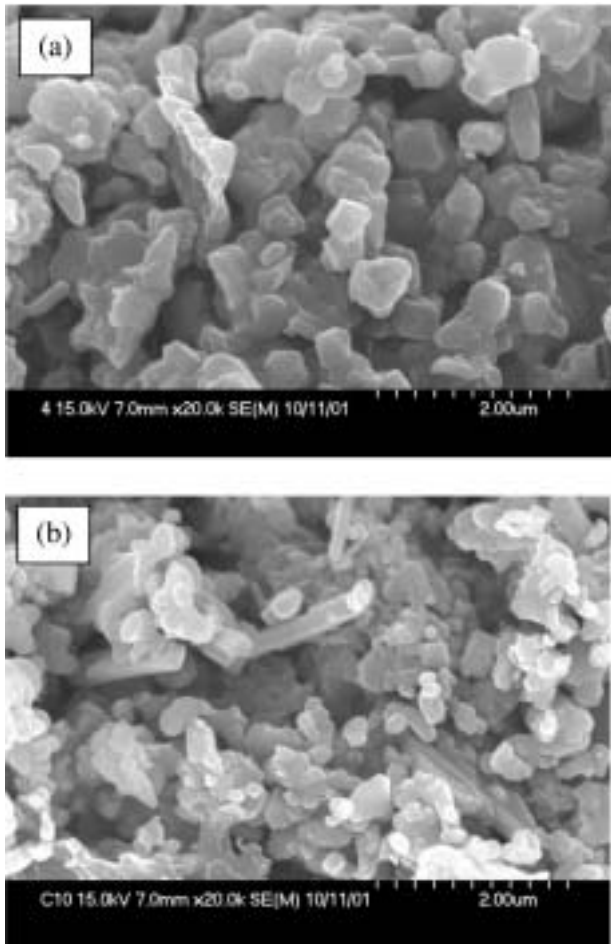

Fig. 3. SEM images for (a) $Li_{0.7}[Li_{1/6}Mn_{5/6}]O_2$ and (b) $Li_{0.7}[Li_{1/12}Ni_{1/12}Mn_{5/6}]O_2$ powders.

Fig. 4(a) and (b) present charge/discharge curves with their discharge capacities for $Li/Li_{0.7}[Li_{1/6}Mn_{5/6}]O_2$ and $Li/Li_{0.7}[Li_{1/12}Ni_{1/12}Mn_{5/6}]O_2$ cells, respectively. The shape of discharge curve at initial cycle for both the electrodes is very similar to that of layered structure. However, the structure of the electrode materials begins to transfer from layered to spinel structures with increasing the cycle number. For $Li_{0.7}[Li_{1/6}Mn_{5/6}]O_2$, especially, the rapid capacity fading is observed in the 3 V region. Similar capacity fading was observed in our previous work [Park et al., 2002]. The $Li/Li_{0.7}[Li_{1/6}Mn_{5/6}]O_2$ cell showed the discharge curve shape similar to that observed from spinel like structure after the 1st cycle. The typical spinel structure shows that the charge/discharge curve shape in the 3 V region is clearly distinct from that in the 4 V region [Thakeray, 1997]. This indicates that $Li_{0.7}[Li_{1/6}Mn_{5/6}]O_2$ undergoes a phase transformation from layered to spinel structure during the cycling. Robertson et al. [2001] also observed the discharge capacity fading of $LiMnO_2$ layered structure due to the transformation of the structure from layered to spinel with cycling. However, $Li_{0.7}[Li_{1/12}Ni_{1/12}Mn_{5/6}]O_2$ shows electrochem-

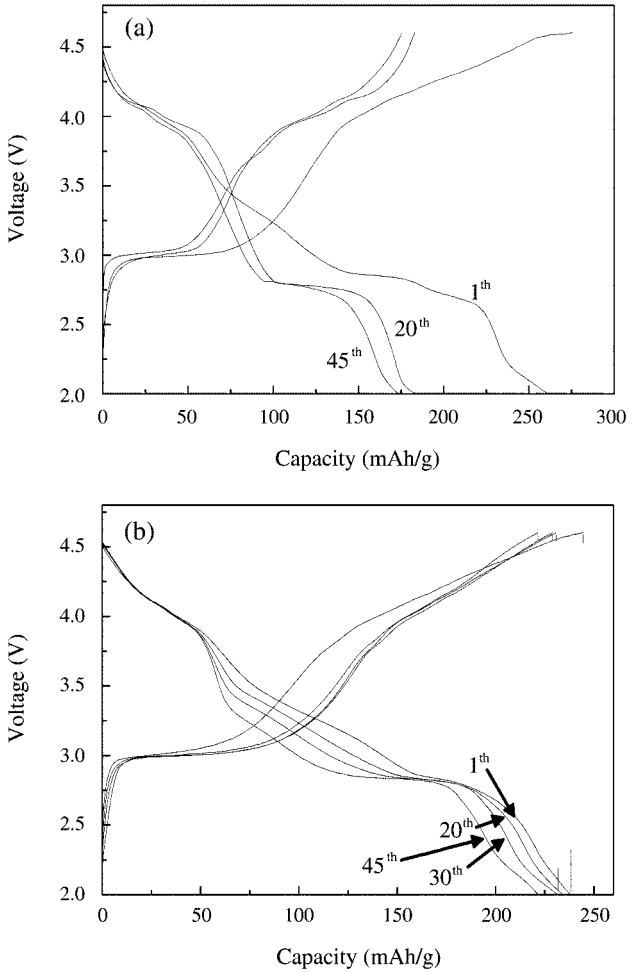

Fig. 4. Charge-discharge curves for (a) $Li_{0.7}[Li_{1/6}Mn_{5/6}]O_2$ and (b) $Li_{0.7}[Li_{1/12}Ni_{1/12}Mn_{5/6}]O_2$.

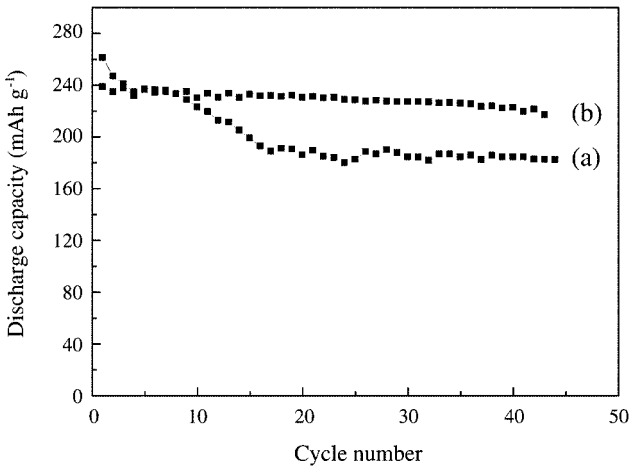

Fig. 5. Plots of specific discharge capacity versus cyclic number for (a) $Li_{0.7}[Li_{1/6}Mn_{5/6}]O_2$ and (b) $Li_{0.7}[Li_{1/12}Ni_{1/12}Mn_{5/6}]O_2$.

ical characteristics slightly different from $Li_{0.7}[Li_{1/6}Mn_{5/6}]O_2$. The sample represents that the discharge curve initially appears as if the material has a layered structure, but the sample transits from layered to spinel structures with cycling, as observed from $Li_{0.7}[Li_{1/6}Mn_{5/6}]O_2$. However, the discharge capacity fading with the cycle number is significantly reduced in $Li_{0.7}[Li_{1/12}Ni_{1/12}Mn_{5/6}]O_2$. This is because the discharge capacity in the 3 V region, which showed the rapid fading in $Li_{0.7}[Li_{1/6}Mn_{5/6}]O_2$, slightly fades in $Li_{0.7}[Li_{1/12}Ni_{1/12}Mn_{5/6}]O_2$ with increasing the cycle number.

Fig. 5 shows plots of the discharge capacity measured at room temperature versus cycle number for the fabricated Li/$LiPF_6$-EC/DMC (1 : 2 by vol)/Li/$Li_{0.7}[Li_{1/6}Mn_{5/6}]O_2$ and $Li_{0.7}[Li_{1/12}Ni_{1/12}Mn_{5/6}]O_2$ cells. The capacity was measured in the potential range of 2.0-4.6 V at room temperature. Li/$Li_{0.7}[Li_{1/6}Mn_{5/6}]O_2$ and $Li_{0.7}[Li_{1/12}Ni_{1/12}Mn_{5/6}]O_2$ cells initially deliver discharge capacities of 261 and 238 mAh/g, respectively. However, the capacity of $Li_{0.7}[Li_{1/6}Mn_{5/6}]O_2$ and $Li_{0.7}[Li_{1/12}Ni_{1/12}Mn_{5/6}]O_2$ gradually decreases with the cycle number to be 174 and 221 mAh/g after the 45th cycle, respectively. The capacity fading ratio of $Li_{0.7}[Li_{1/12}Ni_{1/12}Mn_{5/6}]O_2$ is lower than that of $Li_{0.7}[Li_{1/6}Mn_{5/6}]O_2$.

It is seen from Fig. 4 that the discharge capacity fading mostly appears in the 3 V region. This charge/discharge behavior is similar to that of $Li_xMn_yO_2$ reported by Armstrong et al. [2002]. They reported that the insertion of lithium into regular spinel at 3 V forms the tetragonal phase and a cubic/tetragonal phase boundary moves in the particles. The formation of the tetragonal phase generates a volume expansion, approximately 6% larger than the cubic phase, and the expansion is anisotropic with a c/a ratio for the tetragonal phase, resulting in the development of a strain in the crystallites. When layered lithium manganese oxides convert to a spinel-like phase, they generate a nanostructure within the particles. The original particles remain larger intact and continue to be pulverized into micrometer dimensions inside. The particles contain a mosaic or a nanograin structure within them. The authors insisted that the formation of the nanograin structure by this way reduces discharge capacity fading. A similar structure has been observed when orthorhombic $LiMnO_2$ converts to spinel with cycling [Armstrong et al., 2002] and for aluminum doped layered materials [Jang et al., 1999; Chiang et al., 2001]. Studies have also discussed the crystallography of the transformation. They detected that, on insertion of lithium into the spinel-like material, the small grains, typically with dimensions of around 60 Å, can distort phases with the strain of the transformation being accommodated by slippage at the grain wall boundaries. As a result, the reduction of the discharge capacity is considered to be due to the formation of nanostructures in the original particles by the first-order phase transformation between undistorted and Jahn-Teller distorted materials.

As discussed above, if the nanograin structure, which decreases discharge capacity fading, initially forms, the capacity fading of the sample might be suppressed. In this work, we synthesized $Li_{0.7}[Li_{1/12}Ni_{1/12}Mn_{5/6}]O_2$ powders consisted of nanograins using a sol-gel method. Fig. 6 shows the nanograins in the $Li_{0.7}[Li_{1/12}Ni_{1/12}Mn_{5/6}]O_2$ powders. The nanograin structure is apparently observed at magnified SEM image of one particle. In the case of $Li_{0.7}[Li_{1/6}Mn_{5/6}]O_2$, the same result was also observed. It seems that the synthesis of nanostructured particles affords the formation of high surface area necessary for Li ion reaction, resulting in that both the samples deliver high initial discharge capacity. However, the capacity fading rapidly progressed for $Li_{0.7}[Li_{1/6}Mn_{5/6}]O_2$, but not for $Li_{0.7}[Li_{1/12}Ni_{1/12}Mn_{5/6}]O_2$. Ammundsen et al. [2001] reported that nanoparticles would produce a high surface area, but they lead to capacity fade because of the catalytic nature of the manganese oxide surface toward electro-

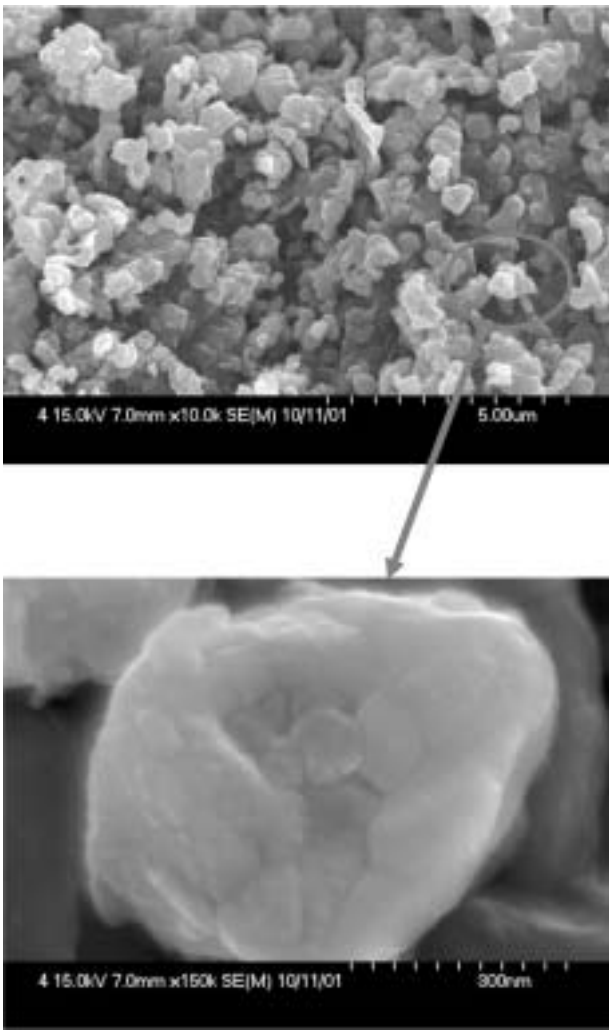

Fig. 6. Magnified SEM image of a $Li_{0.7}[Li_{1/12}Ni_{1/12}Mn_{5/6}]O_2$ particle.

chemical oxidation. However, in the case of $Li_{0.7}[Li_{1/12}Ni_{1/12}Mn_{5/6}]O_2$, although the sample forms nanostructure, capacity fading does not significantly appear. This can be explained with the change of manganese oxidation state with cycling. $Li_{0.7}[Li_{1/6}Mn_{5/6}]O_2$ cannot control the change of manganese oxidation state from Mn^{4+} to Mn^{3+} during the insertion of Li because it includes only Li whose oxidation state is +1. The progress of the charge/discharge processes increases the population of Mn^{3+} in the structure and the discharge capacity rapidly fades due to Jahn-Teller-distortion induced by the phase transition. In the case of Ni-doped $Li_{0.7}[Li_{1/12}Ni_{1/12}Mn_{5/6}]O_2$, however, the transition of Mn^{4+} to Mn^{3+} will begin after all Ni4+ are totally reduced into Ni^{2+} during the charge process. This suppresses the phase transition from Mn^{4+} to Mn^{3+}, which generates the Jahn-Teller-distortion. This phenomenon is able to reduce the rapid capacity fading induced during the charge/discharge processes. Consequently, in this work, we were able to synthesize the $Li_{0.7}[Li_{1/12}Ni_{1/12}Mn_{5/6}]O_2$ powders consisting of various nanometer-sized nanograins using a sol-gel method at low temperature and could suppress the change of Mn oxidation state by Ni-doping. This enables the $Li_{0.7}[Li_{1/12}Ni_{1/12}Mn_{5/6}]O_2$ to deliver high initial discharge capacity while it retains low capacity fading.

CONCLUSION

$Li_{0.7}[Li_{1/6}Mn_{5/6}]O_2$ and $Li_{0.7}[Li_{1/12}Ni_{1/12}Mn_{5/6}]O_2$ powders were synthesized by using a sol-gel method. The powders had a typical rhombohedral layered O3 structure, and the a/c ratios of $Li_{0.7}[Li_{1/6}Mn_{5/6}]O_2$ and $Li_{0.7}[Li_{1/12}Ni_{1/12}Mn_{5/6}]O_2$ were 5.02 and 5.15, respectively. Both the samples showed the nanograin structure observed at a magnified SEM image of one particle. The particle size of $Li_{0.7}[Li_{1/12}Ni_{1/12}Mn_{5/6}]O_2$ (300 nm) was smaller than that of $Li_{0.7}[Li_{1/6}Mn_{5/6}]O_2$ (500 nm). Li/$Li_{0.7}[Li_{1/6}Mn_{5/6}]O_2$ and $Li_{0.7}[Li_{1/12}Ni_{1/12}Mn_{5/6}]O_2$ cells initially delivered discharge capacities of 261 and 238 mAh/g, respectively. However, the capacities gradually decreased with the cycle number to be 174 and 221 mAh/g after the 45th cycle, respectively. It was concluded which is nanometer sized nanograins and suppress the change of Mn oxidation state by Ni-doping in $Li_{0.7}[Li_{1/12}Ni_{1/12}Mn_{5/6}]O_2$. $Li_{0.7}[Li_{1/12}Ni_{1/12}Mn_{5/6}]O_2$ delivered high initial discharge capacity while retaining low capacity fading.

ACKNOWLEDGMENT

This work was supported by the Ministry of Science and Technology, Korea.

REFERENCES

Ammundsen, B. and Paulsen, J., "Novel Lithium-Ion Cathode Materials Based on Layered Manganese Oxides," *Adv. Mater.*, **13**, 943 (2001).

Ammundsen, B., Desilvestro, J., Groutso, T., Hassell, K., Metson, J. B., Regan, E., Steiner, R. and Pickering, P., "Synthesis and Electrochemical Studies of Spinel Phase $LiMn_2O_4$ Cathode Materials Prepared by the Pechini Process," *J. Electrochem. Soc.*, **143**, 879 (1996).

Armstrong, A. R., Huang, H., Jennings, R. A. and Bruce, P. G., "$Li_{0.44}MnO_2$ an Intercalation Electrode with a Tunnel Structure and Excellent Cyclability," *J. Mater. Chem.*, **8**, 255 (1998).

Armstrong, A. R., Paterson, A. J., Robertson, A. D. and Bruce, P. G., "Nonstoichiometric Layered $Li_xMn_yO_2$ with a High Capacity for Lithium Intercalation/Deintercalation," *Chem. Mater.*, **14**, 710 (2002).

Armstrong, A. R., Robertson, A. D., Gitzendanner, R. and Bruce, P. G., "The Layered Intercalation Compounds $Li(Mn_{1-y}Co_y)O_2$: Positive Electrode Materials for Lithium-Ion Batteries," *J. Solid State Chem.*, **145**, 549 (1999).

Bruce, P. G., Armstrong, A. R. and Gitzendanner, R. L., "New Intercalation Compounds for Lithium Batteries: Layered $LiMnO_2$," *J. Mater. Chem.*, **9**, 193 (1999).

Bruce, P. G., Armstrong, A. R. and Gitzendanner, R. L., "New Intercalation Compounds for Lithium Batteries: Layered $LiMnO_2$," *J. Mater. Chem.*, **9**, 193 (1999).

Chiang, Y. M., Wang, H. and Jang, Y. I., "Electrochemically Induced Cation Disorder and Phase Transformations in Lithium Intercalation Oxides," *Chem. Mater.*, **13**, 53 (2001).

Choi, S. and Manthiram, A., "Factors Influencing the Layered to Spinel-like Phase Transition in Layered Oxide Cathodes," *J. Electrochem. Soc.*, **149**, A1157 (2002).

Crohuennec, L., Deniard, P. and Brec, R., "Electrochemical Cyclability of Orthorhombic $LiMnO_2$. Characterization of Cycled Materials," *J. Electrochem. Soc.*, **144**, 3323 (1997).

Davidson, I. J., McMillan, R. J. and Greedan, J. E., "Lithium-ion Cell Based on Orthorhombic $LiMnO_2$," *J. Power Sources*, **54**, 232 (1995).

Davidson, I. J., McMillan, R. J., Slegr, H., Luan, B., Kargina, I., Murray, J. J. and Swainson, I. P., "Electrochemistry and Structure of $Li_{2-x}Cr_yMn_{2-y}O_4$ Phases," *J. Power Sources*, **82**, 406 (1999).

Holzapel, M., Haak, C. and Ott, J. A., "Lithium-Ion Conductors of the System $LiCo_{1-x}Fe_xO_2$, Preparation and Structural Investigation," *Solid State Chemistry*, **156**, 470 (2001).

Kang, S. G., Kang, S. Y., Ryu, K. S. and Chang, S. H., "Electrochemical and Structural Properties of HT-$LiCoO_2$ and LT-$LiCoO_2$ Prepared by the Citrate Sol-gel Method," *Solid State Ionics*, **120**, 155 (1999).

Lee, Y. S., Sun, Y. K. and Nahm, K. S., "Synthesis and Characterization of $LiNiO_2$ Cathode Material Prepared by an Adiphic Acid-assisted Sol-gel Method for Lithium Secondary Batteries," *Solid State Ionics*, **118**, 159 (1999).

Lide, D. R., "CRC HANDBOOK of CHEMISTRY and PHYSICS," 74th Edition, Boca Raton, FL.

Lu, Z. and Dahn, J. R., "Understanding the Anomalous Capacity of Li/$Li[Ni_xLi_{(1/3-2x/3)}Mn_{(2/3-x/3)}]O_2$ Cells Using *In Situ* X-Ray Diffraction and Electrochemical Studies," *J. Ecs*, **149**, A815 (2002).

Lu, Z., Donaberger, R. A. and Dahn, J. R., "Superlattice Ordering of Mn, Ni, and Co in Layered Alkali Transition Metal Oxides with P2, P3, and O3 Structures," *Chem. Mater.*, **3583**, 12 (2000).

Park, K. S., Cho, M. H., Park, S. H., Nahm, K. S., Sun, Y. K., Lee, Y. S. and Yoshio, M., "The Effects of Ni and Li Doping on the Performance of Lithium Manganese Oxide Material for Lithium Secondary Batteries," *Electrochim. Acta*, **47**, 2937 (2002).

Park, S. H., Park, K. S., Cho, M. H., Sun, Y. K., Nahm, K. S., Lee, Y. S. and Yoshio, M., "The Effects of Oxygen Flow Rate and Anion Doping on the Performance of the $LiNiO_2$ Electrochemical for Lithium Secondary Batteries," *Korean J. Chem. Eng.*, **19**, 791 (2002).

Park, S. H., Park, K. S., Sun, Y. K., Nahm, K. S., Lee, Y. S. and Yoshio, M., "Structural and Electrochemical Characterization of Lithium Excess and Al-doped Nickel Oxides Synthesized by the Sol-gel Method," *Electrochem. Acta*, **46**, 1215 (2001).

Park, S. H., Sun, Y.-K., Park, K. S., Nahm, K. S., Lee, Y. S. and Yoshio, M., "Synthesis and Electrochemical Properties of Lithium Nickel Oxysulfide ($LiNiS_yO_{2-y}$) Material for Lithium Secondary Batteries," *Electrochem. Acta*, **47**, 1721 (2002).

Paulsen, J. M. and Dahn, J. R., "O_2-Type $Li_{2/3}[Ni_{1/3}Mn_{2/3}]O_2$: A New Layered Cathode Material for Rechargeable Lithium Batteries II. Structure, Composition, and Properties," *J. Electrochem. Soc.*, **2478**, 147 (2000).

Paulsen, J. M., Larcher, D. and Dahn, J. R., "O2 Structure $Li_{2/3}[Ni_{1/3}Mn_{2/3}]O_2$: A New Layered Cathode Material for Rechargeable Lithium Batteries III. Ion Exchange," *J. Electrochem. Soc.*, **2862**, 147 (2000).

Paulsen, J. M., Muller-Neuhaus, J. R. and Dahn, J. R., "Layered $LiCoO_2$ with a Different Oxygen Stacking (O2 Structure) as a Cathode Material for Rechargeable Lithium Batteries," *J. Electrochem. Soc.*, **147**, 508 (2000).

Paulsen, J. M., Thomas, C. L. and Dahn, J. R., "Correlating Capacity Loss of Stoichiometric and Nonstoichiometric Lithium Manganese Oxide Spinel Electrodes with Their Structural Integrity," *J. Electrochem. Soc.*, **146**, 3649 (1999).

Paulsen, J. M., Thomas, C. L. and Dahn, J. R., "Layered Li-Mn-Oxide with the O2 Structure: A Cathode Material for Li-Ion Cells which Does Not Convert to Spinel," *J. Electrochem. Soc.*, **3560**, 146 (1999).

Paulsen, J. M., Thomas, C. L. and Dahn, J. R., "O2 Structure $Li_{2/3}[Ni_{1/3}Mn_{2/3}]O_2$: A New Layered Cathode Material for Rechargeable Lithium Batteries. I. Electrochemical Properties," *J. Electrochem. Soc.*, **147**, 861 (2000).

Robertson, A. D., Armstrong, A. R. and Bruce, P. G., "Layered $Li_xMn_{1-y}Co_yO_2$ Intercalation Electrodes-Influence of Ion Exchange on Capacity and Structure upon Cycling," *Chem. Mater.*, **13**, 2380 (2001).

Sun, Y. K., Kim, D. W., Jin, S. H., Hyung, Y. E., Moon, S. I. and Kim, D. W., "Synthesis and Cycling Behavior of $LiMn_2O_4$ Cathode Materials Prepared by Glycine-assisted Sol-gel Method for Lithium Secondary Balleries," *Korean J. Chem. Eng.*, **15**, 64 (1998).

Sun, Y. K. and Kim, D. W., "Synthesis and Electrochemical Characterization of $LiMn_2O_4$ Cathode Materials for Lithium Polymer Batteries," *Korean J. Chem. Eng.*, **16**, 449 (1999).

Sun, Y. K. and Nahm, K. S., "Electrochemical Properties of Oxysulfide $LiAl_{0.18}Mn_{1.82}O_{3.97}S_{0.03}$ Cathode Materials at Evaluated Temperature," *Korean J. Chem. Eng.*, **19**, 718 (2002).

Thakeray, M. M., "Manganese Oxides for Lithium Batteries," *Prog. Solid St. Chem.*, **25**, 1 (1997).

Wang, H., Jang, Y. I. and Chiang, Y. M., "Origin of Cycling Stability in Monoclinic- and Orthorhombic-Phase Lithium Manganese Oxide Cat," *Electrochem. Solid State Lett.*, **2**, 490 (1999).